Pergamon

Int. J. Solids Structures Vol. 32, No. 8/9, pp. 1307–1318, 1995

0020–7683/95 $9.50 + .00

0020–7683(94)00137–5

FAILURE ANALYSIS OF ROTATING DISKS

CHARLES W. BERT and TAPAN K. PAUL
School of Aerospace and Mechanical Engineering, The University of Oklahoma, Norman, OK 73019, U.S.A.

(*Received* 8 *July* 1993; *in revised form* 3 *June* 1994)

Abstract—Based on the plane elasticity solution, the size and the number of pie-sector shaped fragments produced at the failure of a rotating flat disk have been determined. In the analysis, it is assumed that a radial through-thickness crack has propagated from the bore to some extent, which could be due to the progressive growth of a pre-existing flaw under low-cycle fatigue loading. Taking the crack plane as the plane of symmetry and assuming that the crack length is critical, one-half of the disk has been analysed. At the onset of the unstable propagation of the assumed radial crack, a possible second failure location away from the original crack at the inside boundary of the disk has been determined. The size of the pie-sector shaped fragments as obtained in the analysis has been compared with the available experimental results [Sato and Nagai (1963), National Aerospace Laboratory, Tokyo, NAL TR-38 and NAL TR-47 (in Japanese)]. The results are in close agreement with the experiment. It is noted that, as the ratio of the inner radius to the outer radius of the disk increases, the number of fragments also increases, as it has been observed experimentally. The present analysis technique is suitable for disks having a smaller ratio of inside to outside radii.

1. INTRODUCTION

In the design of containments for rotating disks, it is very important to know the probable size of the fragments which will be thrown at the failure of the disk. As reported by Mangano (1975), 170 rotor failures were experienced in 1973. These failures accounted for approx. 9% of the 2888 shutdowns that were experienced by the gas turbine-powered U.S. commercial aircraft fleet.

The larger the size of the fragments, the more translational energy is possessed by it. The fragment with maximum translational energy is a disk segment subtending an angle of 133.6° (McCarthy, 1975). Experience has shown that, for practical purposes, it is the translational energy that causes the real damage on impact, because the translational energy is in the direction of the impact. McCarthy (1975) has also pointed out that, the larger the fragment size, the greater the possibility of a strike to an aircraft component.

A few rotor burst experiments have been carried out. As an aid to the design of rotor containment rings, Mangano (1975) conducted experiments with rotor failures into six, four, three and two pie-sector shaped fragments, having included angles of 60°, 90°, 120° and 190°, respectively. Sato and Nagai (1963a,b) performed experiments on the bursting of uniform-thickness rotating disks. In their experiments cast iron flat disks of different ratios of γ (ratio of inside radius to outside radius of the disk) were burst into different sizes of fragments. The number of fragments produced at the failure increased with an increase in the ratio γ. However, theoretical studies pertaining to rotor or rotating disk failure are almost absent except the recent works of Köhl and Dhondt (1993) and Bandera *et al.* (1993). In the analysis performed by Köhl and Dhondt (1993) the disk has been modeled as a rotating ring. The resulting stress distribution in the half-ring immediately after a complete radial cracking has been determined by the modal analysis technique. It was shown that the stress distribution can lead to an additional failure at about 120° away from the original crack surface. In the work of Bandera *et al.* (1993), the quasi-static method of analysis based on curved beam theory has been put forward. Ring fragmentation sequence has been interpreted, based on a modified stress distribution after a complete radial cut introducing a dynamic correction factor.

In the present study, the rotating disk has been analysed as a two-dimensional plane-stress elasticity problem, considered as a quasi-static one by virtue of d'Alembert's principle.

In the analysis, it is assumed that a through-thickness radial crack has propagated from the bore to some extent. The crack length is assumed as the critical length. For a *disk*, spinning at very high speed, a part-radial crack could be more appropriate than considering a complete radial crack as the stage for the determination of stress distribution in the disk. However, a complete radial crack was considered in the analysis by Köhl and Dhondt (1993).

At the onset of the unstable propagation of the assumed radial crack, the stress distribution at the inside boundary of the half-disk has been obtained. It is shown that this stress distribution can lead to a second failure at a location away from the original crack along the inside boundary of the disk. The location of failure is dependent on the ratio, γ. The size of the pie-sector shaped fragments obtained in the analysis of cast iron flat disks of different values of γ has been compared with available experimental results obtained by Sato and Nagai (1963a,b). The results obtained in the analysis are in good agreement with the experiments.

2. CONCEPTUAL APPROACH

2.1. *Bursting mechanism*

A flat disk, fitted to the shaft, is rotating steadily at a certain speed ω about an axis perpendicular to the plane of the disk and passing through the shaft center. In the analysis, it is assumed that a through-thickness radial crack has propagated from the bore to some extent, which could be due to the progressive growth of a pre-existing flaw under low-cycle fatigue loading. The tensile circumferential stress acting along the crack plane due to the applied centrifugal loading is shown in Fig. 1. The circumferential stress is replaced by stress resultants P and M', which are also shown in Fig. 1. Note that M' is the moment evaluated about the center of the disk.

The crack length $\bar{a}$ is assumed as the critical length. This means we have to increase speed, and thus the shrink fit pressure decreases. It is assumed that the disk is still intact with the shaft at the critical speed before a complete radial cut or burst occurs. The stress resultants P and M' correspond to the critical condition.

Since the part-through radial crack is critical, its propagation in the radial direction is unstable. As the crack advances in the radial direction, the value of P (critical) changes and acts as an instantaneous fast-moving load on the crack flanks. It could be imagined

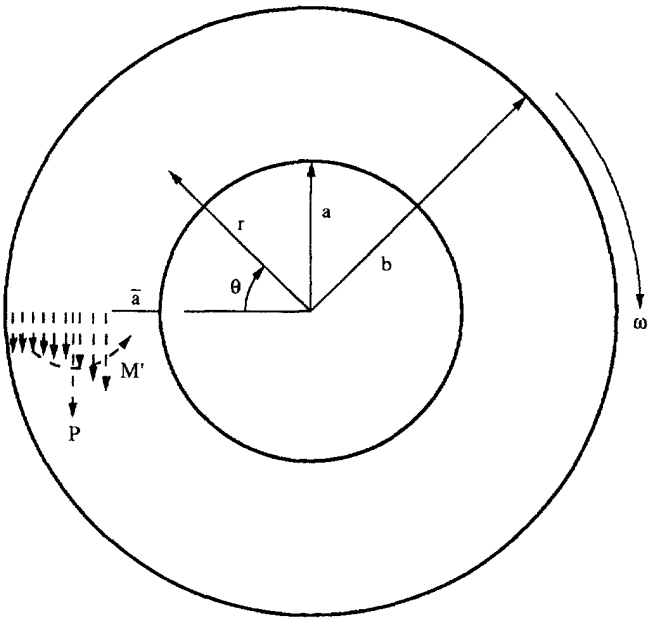

Fig. 1. Rotating disk with a crack.

that the two crack flanks are being pulled apart while the disk is rotating. When the running crack tip reaches the outermost fiber of the disk, it is a complete radial cut. Our objectives are to compute the stress distribution at the onset of the unstable propagation of the assumed radial crack and just after a complete radial crack has occurred. In the first case the crack flank is not load-free, while in the second case it is load-free. The second case is a special case of the first one. It is mentioned that a crack is stable in the structure if it is not propagating, or its growth could be stable depending on the crack-tip plasticity condition. Here we are dealing with the unstable propagation of the crack. In this situation rapid crack propagation occurs and it is not unreasonable to think that the crack flanks are loaded with fast-moving forces which are equal in magnitude to the tensile value at the stable or equilibrated situation, and acting opposite to the tensile direction.

In the first case the part-through radial crack is made a complete crack by applying the circumferential stress resultant P equal in magnitude, but opposite in direction, with corresponding moment M, as shown in Fig. 2. P (critical) is the load considered here, such that unstable propagation has been assumed to have already started so that the quasi-static solution method can be applied. It is assumed that the complete radial cut has occurred at least after a short time (few micro-seconds), during which the inertia effect is predominant. In the second case, $P \approx 0$ and $M \approx 0$ at the instant just after a complete cut. The problem has been solved as a quasi-static plane-stress elasticity problem by virtue of the d'Alembert's principle. From the stress distribution thus obtained, our objective is to find any possible location at the inside boundary of the disk, away from the original crack surface where failure can initiate based on a failure criterion.

The two crack flanks are going to be displaced from each other and the disk shrinks in the circumferential direction. Owing to this radial burst the disk shrinks in the radial direction too from its original, radially expanded position. The outer boundary of the disk shrinks with a certain velocity depending on the rotational speed. This is equivalent to a compressive loading at the outside boundary of the disk. In fact, at the onset of unstable crack propagation the cracked part of the disk shrinks circumferentially. Due to the cutting of tensile hoop fibers of the disk, the outer boundary of the disk moves rapidly inward. This dynamic action is modeled as a quasi-static radial and hoop compressive state of stress. Thus, it can even be thought that the disk outer surface was stress-free before a burst, but dynamically loaded just after the burst, or during the unstable propagation of a part-through radial crack. The disk shrinks in the circumferential direction as well as in the radial direction and simultaneously slides over the shaft. It remains in contact with the shaft as long as the effect of this dynamic loading diminishes.

This approach is believed to be the simplest way to analyse fragmentation of a rotating disk, rather than solving a complicated plane elasto-dynamic crack problem and analysing subsequent dynamic loading of the disk during unstable crack propagation.

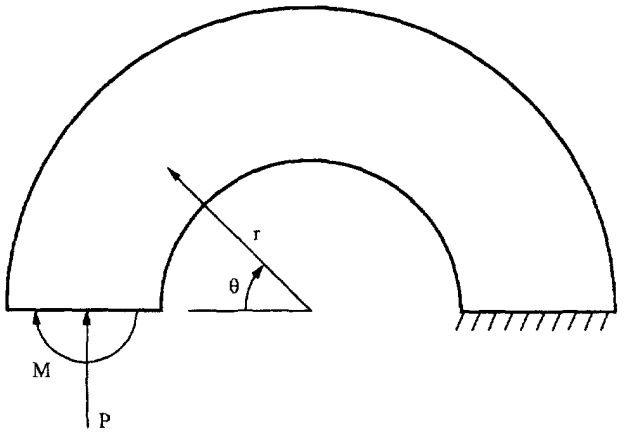

Fig. 2. Half of the disk, showing applied loads.

2.2. *Fragmentation sequence*

According to the analysis, we explain the propagation of failure along the inside boundary of the disk, which breaks into pieces as follows. If crack A is taken along 0°, as shown in Fig. 3, according to our analysis, cracks B and E start to propagate from the bore. As we have explained above, initiation of a crack along the inside boundary of the disk is due to the unstable propagation of another crack; thus, when cracks B and E become critical, cracks C and D start to propagate and lead to complete failure. It is noted that in this paper we have studied only the initiation of a crack along the inside boundary of the disk, not its subsequent propagation, which is greatly influenced by shrinking in the radial direction and somewhat less by centrifugal action. However, in practice in the rotating direction, crack B becomes critical before crack E reaches critical, which is in the direction opposite to the direction of rotation, while crack B is critical, crack C starts and crack D starts relatively later than does C. This can be imagined from Fig. 3 by observing the relative positions of pieces from the center of the shaft. Obviously, these events happen in a very short time.

3. ANALYSIS OF THE DISK

With the crack plane as the plane of symmetry, the half of the disk with polar coordinate system r and θ is shown in Fig. 2. The governing differential equations of equilibrium are as follows:

$$\frac{\partial \sigma_r}{\partial r} + \frac{1}{r}\frac{\partial \tau_{r\theta}}{\partial \theta} + \frac{\sigma_r - \sigma_\theta}{r} + \rho\omega^2 r = 0 \tag{1}$$

$$\frac{1}{r}\frac{\partial \sigma_\theta}{\partial \theta} + \frac{\partial \tau_{r\theta}}{\partial r} + \frac{2\tau_{r\theta}}{r} = 0. \tag{2}$$

In the above equations σ_r, σ_θ and $\tau_{r\theta}$ are the radial, circumferential and shear stress components, ρ is the density of the material of the disk and ω is the speed at which the disk is rotating. In terms of the Airy stress function, ϕ, the stress components which satisfy the above equilibrium equations are

$$\begin{aligned} \sigma_r &= \frac{1}{r}\frac{\partial \phi}{\partial r} + \frac{1}{r^2}\frac{\partial^2 \phi}{\partial \theta^2} \\ \sigma_\theta &= \frac{\partial^2 \phi}{\partial r^2} + \rho\omega^2 r^2 \\ \tau_{r\theta} &= \frac{1}{r^2}\frac{\partial \phi}{\partial \theta} - \frac{1}{r}\frac{\partial^2 \phi}{\partial r \partial \theta}. \end{aligned} \tag{3}$$

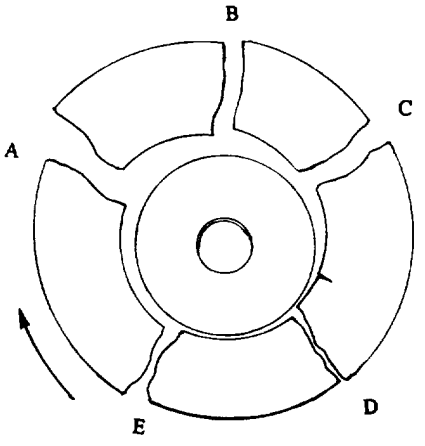

Fig. 3. Fragmented disk, $\gamma = 0.4$ sketched from Sato and Nagai (1963b).

Assuming isotropic material, the strain compatability equation can be written as

$$\left(\frac{\partial^2}{\partial r^2}+\frac{1}{r}\frac{\partial}{\partial r}+\frac{1}{r^2}\frac{\partial^2}{\partial\theta^2}\right)\left(\frac{\partial^2\phi}{\partial r^2}+\frac{1}{r}\frac{\partial\phi}{\partial r}+\frac{1}{r^2}\frac{\partial^2\phi}{\partial\theta^2}\right)=-2(3+\nu)\rho\omega^2. \tag{4}$$

In eqn (4), ν is the Poisson's ratio of the disk material. The expression for ϕ which satisfies the compatability equation is

$$\phi=\left(Ar^3+\frac{B}{r}+Cr+Dr\log r\right)\cos\theta-\frac{1}{32}(3+\nu)\rho\omega^2r^4. \tag{5}$$

Thus, the expressions for stresses become

$$\begin{aligned}\sigma_r&=\left(2Ar-\frac{2B}{r^3}+\frac{D}{r}\right)\cos\theta-\frac{3+\nu}{8}\rho\omega^2r^2\\ \sigma_\theta&=\left(6Ar+\frac{2B}{r^3}+\frac{D}{r}\right)\cos\theta-\frac{1+3\nu}{8}\rho\omega^2r^2\\ \tau_{r\theta}&=\left(2Ar-\frac{2B}{r^3}+\frac{D}{r}\right)\sin\theta.\end{aligned} \tag{6}$$

The three constants A, B and D are evaluated from the following boundary conditions:

$$\text{(a)}\int_a^b\sigma_\theta r\,dr=-M,\quad\text{(b)}\int_a^b\sigma_\theta\,dr=-P\quad\text{at}\quad\theta=0,\quad\text{(c)}\,\tau_{r\theta}=0\quad\text{at}\quad r=b. \tag{7}$$

Boundary conditions (a) and (b), if $M\approx 0$ and $P\approx 0$, respectively, correspond to the condition just after a complete radial cut. The expressions for the constants A, B and D are given as follows:

$$A=\frac{C_mX_p-C_pX_m-MX_p+PX_m}{b^4(2Y_mX_p-Y_pX_m)}-\frac{C_mY_p-2C_pY_m-MY_p+2PY_m}{2b^2(X_mY_p-2X_pY_m)}$$

$$B=\frac{C_mX_p-C_pX_m-MX_p+PX_m}{2Y_mX_p-Y_pX_m}$$

$$D=\frac{C_mY_p-2C_pY_m-MY_p+2PY_m}{X_mY_p-2X_pY_m}$$

where

$$X_m=(b-a)-\frac{b^3-a^3}{b^2},$$

$$Y_m=\frac{b-a}{ab}+\frac{b^3-a^3}{b^4},$$

$$X_p=\log\frac{b}{a}-\frac{3(b^2-a^2)}{2b^2},$$

$$Y_p=\frac{3(b^2-a^2)}{b^4}+\frac{b^2-a^2}{a^2b^2},$$

$$C_m = \frac{1+3\nu}{32}\rho\omega^2(b^4 - a^4),$$

$$C_p = \frac{1+3\nu}{24}\rho\omega^2(b^3 - a^3).$$

For an assumed radial crack of length $\bar{a}$, as the critical length in a disk with specified radii r_1, r_2, and the thickness, the magnitude of the force P in eqn (7) has been estimated as the load required to have unstable propagation of a crack of the same size in an arc-shaped specimen, as shown in Fig. 4. The specimen shown in Fig. 4 is the ASTM standard specimen and is specified in E399 (ASTM, 1987) for plane-strain fracture toughness test using a C-shaped specimen. The expression for the stress intensity factor is given below. For the present purpose, K_Q is replaced with the material fracture toughness, K_{Ic}. Thus, from eqn (8), an estimate of the load P can be obtained.

$$K_Q = \frac{P}{tW^{1/2}}\left[3\frac{X}{W} + 1.9 + 1.1\frac{\bar{a}}{W}\right]\left[1.0 + 0.25\left(1.0 - \frac{\bar{a}}{W}\right)^2\left(1.0 - \frac{r_1}{r_2}\right)\right] f\left(\frac{\bar{a}}{W}\right), \tag{8}$$

where

$$f\left(\frac{\bar{a}}{W}\right) = \left[\frac{\left(\frac{\bar{a}}{W}\right)^{1/2}}{\left(1.0 - \frac{\bar{a}}{W}\right)^{3/2}}\left(3.74 - 6.30\frac{\bar{a}}{W} + 6.32\left(\frac{\bar{a}}{W}\right)^2 - 2.43\left(\frac{\bar{a}}{W}\right)^3\right)\right].$$

Where $\bar{a}$ is the crack length, t is the specimen thickness, P is the applied load, and W is the specimen width.

With reference to Fig. 1, $r_1 = a$ and $r_2 = b$. The above parameters appearing in eqn (8) are shown in Fig. 4. The magnitude of M is estimated as $P(a+b)/2$. It is noted that the accuracy of eqn (8) in evaluating K_Q for all values r_1/r_2 is considered to be $\pm 3\%$ for $0.2 \leqslant \bar{a}/W \leqslant 1.0$ and $0 \leqslant X/W \leqslant 1$.

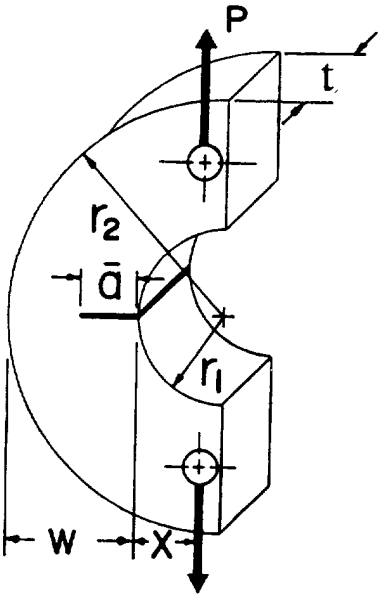

Fig. 4. Specimen indicating geometric parameters.

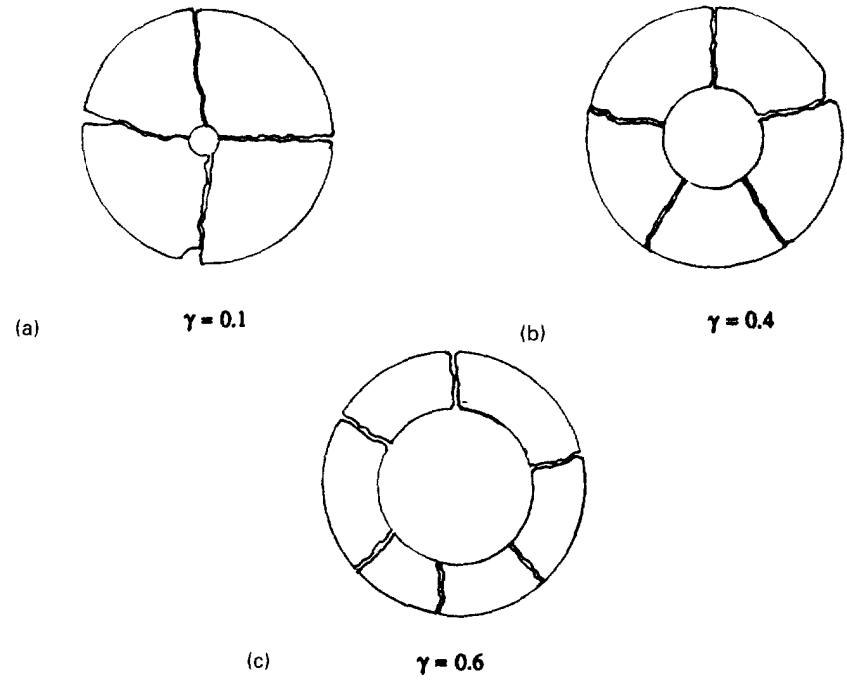

Fig. 5. Schematic diagrams of fracture patterns from Sato and Nagai (1963b).

4. EXAMPLE, RESULTS AND DISCUSSIONS

The above analysis is applied to cast iron flat disks of different ratios of inside to outside radii, γ. The material properties of the disk are density, $\rho = 0.26$ lb in^{-3}, ultimate tensile strength, $\sigma_{ut} = 43.0$ ksi, Poisson's ratio, $\nu = 0.21$, and plane-strain fracture toughness, $K_{Ic} = 40.0$ ksi$\sqrt{\text{in}}$ (*Metals Handbook*, 1990). Estimated values of applied loads P and M are tabulated in Table 1.

The stress distribution is shown in Fig. 6, $\gamma = 0.1$. From the distribution of the von Mises effective stress, it is evident that, during the unstable propagation of the assumed crack in the radial direction, a second radial crack could initiate at the location $\theta = 90°$ from the original crack at the inside boundary of the disk, by reaching the ultimate tensile strength of the material. The ultimate tensile strength is 43 ksi for this cast iron disk. During the propagation of the second radial crack a third one could be expected to initiate at 180°, thus propagating failure of the disk into fragments of equal size. The disk would be expected to fail into four fragments. The four pie-sector shaped fragments produced at the failure of the same cast iron disk in the experiment is shown in Fig. 5(a). The fragments are almost equal in size. The critical speed ω_c is found to be almost 10,828 rpm. The stress distribution at the inside boundary at the speed level lower than the above critical value is safe when compared to ultimate tensile strength. The above analysis also predicts a safe speed for a disk with a specified radial crack extended from the hub.

The result shown in Fig. 7 is for a disk with $\gamma = 0.3$. The result is similar to $\gamma = 0.1$, as discussed above. Figure 8 illustrates the stress distribution for a disk with $\gamma = 0.4$. The fragment size is found to have an included angle of 83°. In this case, the disk would be

Table 1. Estimates for applied loads P and M

$\gamma = r_1/r_2$	$\bar{a}/W$	X/W	P (kips/in.)	M (kip-in./in.)
0.1	0.5	0.11	7.73	21.25
0.3	0.5	0.43	5.14	16.70
0.4	0.5	0.66	4.02	14.07
0.5	0.5	1.00	3.02	11.32
0.6	0.5	1.50	2.12	8.48

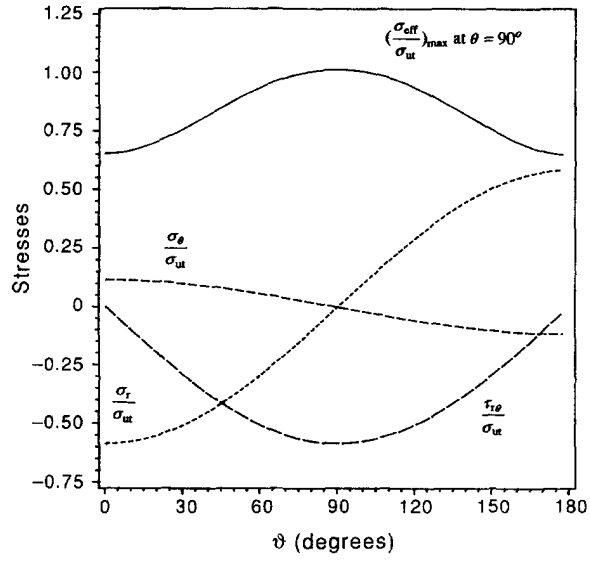

Fig. 6. Stress pattern in the half-disk. (Material: cast iron, $\gamma = 0.1$, $\bar{a}/W = 0.5$, critical speed, $\omega_c = 10{,}828$ rpm.)

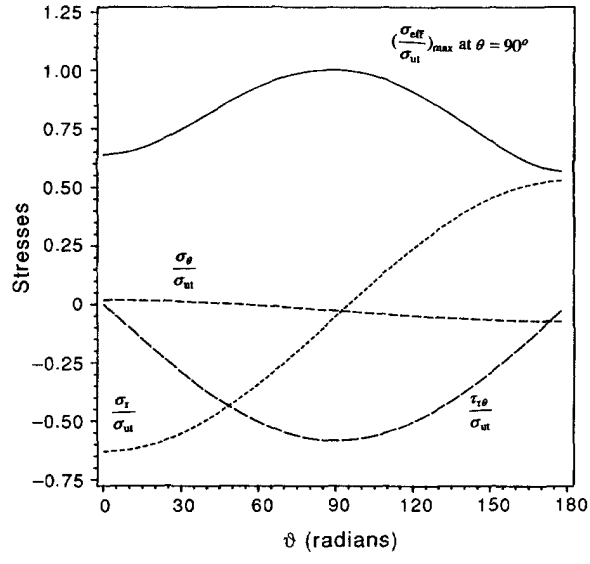

Fig. 7. Stress pattern in the half-disk. (Material: cast iron, $\gamma = 0.3$, $\bar{a}/W = 0.5$, critical speed, $\omega_c = 17{,}665$ rpm.)

expected to fail into almost four or five pie-sector shaped fragments. Figure 9 illustrates the stress distribution for a disk with $\gamma = 0.5$. The von Mises effective stress peaks up at 74°. In this case, the disk is expected to fail into five equal pie-sector shaped fragments. In Fig. 5(b), the number of fragments obtained in the experiment is five for a disk of $\gamma = 0.4$. Figure 10 illustrates the stress distribution along the inside boundary of the disk with $\gamma = 0.1$ just after a complete radial cracking has occurred. In this case, $P \approx 0$ and $M \approx 0$. The location of a second crack initiation from the original crack along the inside boundary of the disk is the same as that for a part-through crack in Fig. 6. It is evident that the location of crack initiation along the inside boundary of the disk does not change whether it is a part-through crack or almost a complete radial crack. Figures 11 and 12 illustrate similar results for the cases $\gamma = 0.3$ and 0.5, respectively.

From the experimental results in Fig. 5(a)–(c), it is ascertained that the number of fragments produced at the failure increases with an increase in ratio γ. The same result is obtained in the analysis for disks with $\gamma = 0.1$, 0.3, 0.4 and 0.5. However, it should be

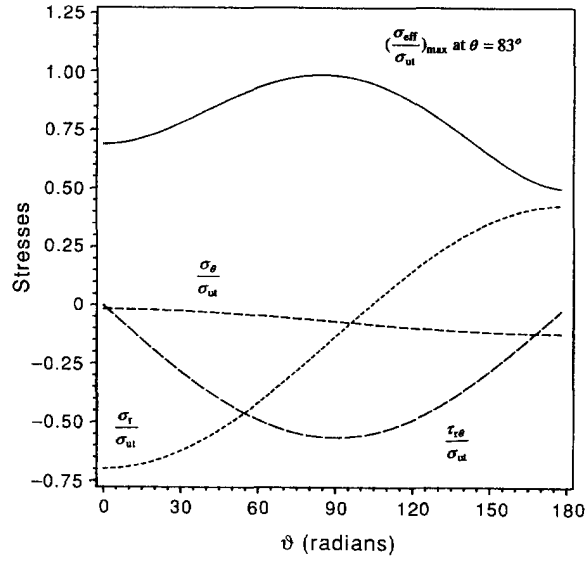

Fig. 8. Stress pattern in the half-disk. (Material: cast iron, $\gamma = 0.4$, $\bar{a}/W = 0.5$, critical speed, $\omega_c = 22{,}010$ rpm.)

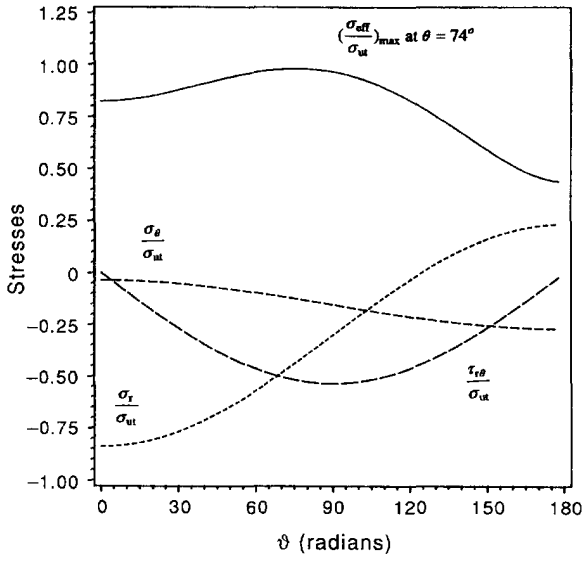

Fig. 9. Stress pattern in the half-disk. (Material: cast iron, $\gamma = 0.5$, $\bar{a}/W = 0.5$, critical speed, $\omega_c = 26{,}546$ rpm.)

mentioned here that in the result obtained from the method of analysis adopted, as well as in the result obtained in the bursting test of a flat rotating disk of cast iron (Sato and Nagai, 1963a,b), we could not obtain a disk failed into three equal pie-sector shaped fragments.

In the analysis, we have adopted the von Mises effective stress as the failure criterion. It could be argued that the maximum principal stress criterion would be appropriate in this case. "Under more complicated conditions, such as the multiaxial stressing of a turbine disk, it is frequently customary to assume that the failure criterion is based on the octahedral shear stress (τ_{oct}) containing all three principal stresses, (σ_i)" (Williams, 1974). The application of the maximum principal stress criterion in this situation turns out to be treating the fracture of a small material element of the disk similar to the uniaxial case. It is evident from our analysis that the maximum tensile principal stress always occurs at about 120° for $\gamma = 0.1$–0.5, which implies failure of the disk into three equal pie-sector shaped fragments. The uniaxial treatment of the problem has been demonstrated by Köhl and Dhondt (1993). They have addressed failure of the disk into three equal pie-sector shaped fragments

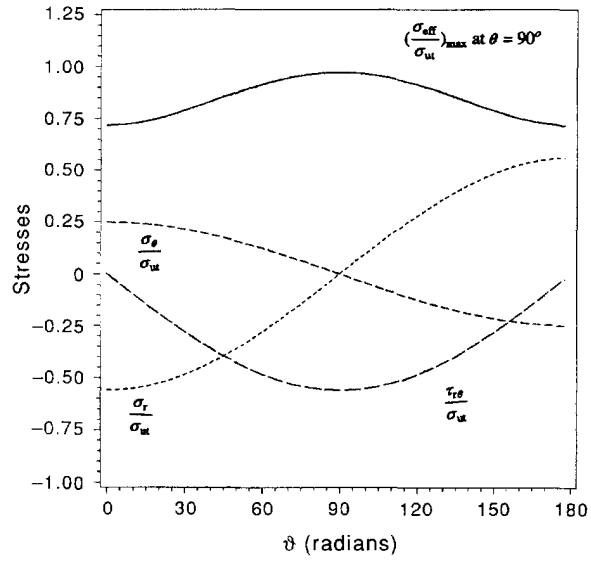

Fig. 10. Stress pattern in the half-disk. (Material: cast iron, $\gamma = 0.1$, $\bar{a}/W = 1.0$, critical speed, $\omega_c = 5{,}060$ rpm.)

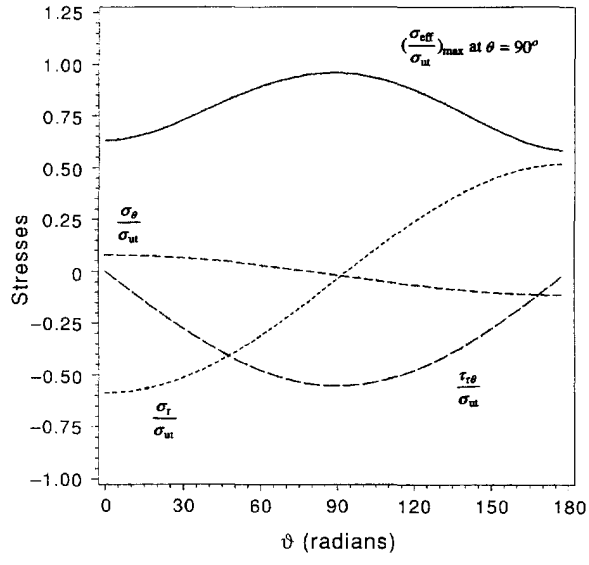

Fig. 11. Stress pattern in the half-disk. (Material: cast iron, $\gamma = 0.3$, $\bar{a}/W = 1.0$, critical speed, $\omega_c = 15{,}135$.)

by the modal analysis technique. It is mentioned here that a flat disk broken into three fragments has been observed neither in our analysis nor in the experimental work of Sato and Nagai (1963a,b). It is apparent that the combination of principal stresses in the failure criterion plays an important role in locating the positions of failures. This has also been mentioned in the monograph by Gdoutos (1984).

In this plane stress treatment of the cast iron flat disk, as long as the fracturing element has sufficient tensile principal stress with the other principal stress compressive, then the von Mises criterion is appropriate. It predicts the experimental results successfully. In assessing the location of failure, most of the contribution comes from the shear stress. With $\gamma = 0.6$, the disk breaks into six equal pie-sector shaped fragments, as observed in the experiment [Fig. 5(c)]. In this case, the maximum stress occurs at an angle of 40° and both the principal stresses are negative for this cast iron disk, which is inappropriate. The maximum principal stress occurs at 90°, which is at a different location compared to the cases for $\gamma = 0.1$–0.5. As mentioned earlier, the present analysis technique is not appropriate

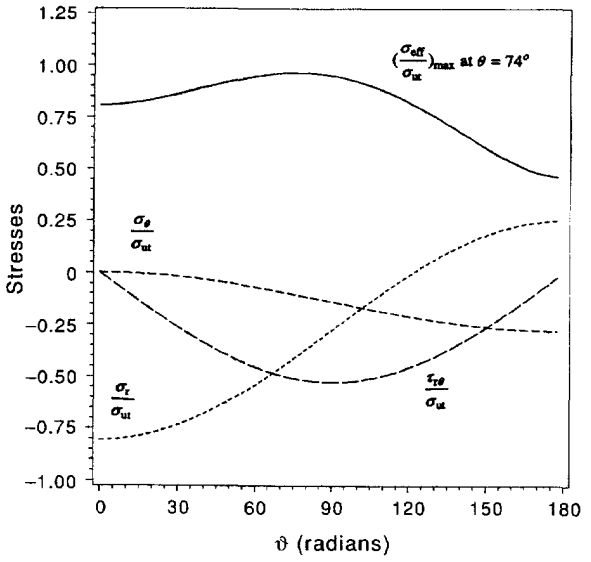

Fig. 12. Stress pattern in the half-disk. (Material: cast iron, $\gamma = 0.5$, $\bar{a}/W = 1.0$, critical speed, $\omega_c = 25{,}400$ rpm.)

for disks with higher values of γ, the ratio of inside to outside radii. At higher values of γ, crack initiation along the inside boundary of the disk becomes a competing situation with compressive hoop stress.

The above analysis has also been applied to a rotor forging steel 4340 disk. The material of the disk is specified as SNCM8 in the Japanese Industrial Standards (JIS). The material properties of the disk are mentioned in Fig. 13. In the reference, the speed at which crack growth of 0.037 in. was observed in the experiment, from a pre-crack of length $\bar{a}/W = 0.17$, was 23,020 rpm. The speed at burst was 26,320 rpm (Sakata *et al.*, 1985). Their predicted crack initiation speed was 22,400 rpm based on J_{Ic} (Rice's J-integral) (Sakata *et al.*, 1978) determined from the ASTM standard compact tension specimen. The critical speed as obtained from the present analysis is 22,870 rpm. According to our analysis, as the crack initiates, the disk will fail within a few cycles. In the present analysis $\bar{a}/W = 0.20$ is taken, owing to the limitations in calculating critical load from eqn (8). Unfortunately,

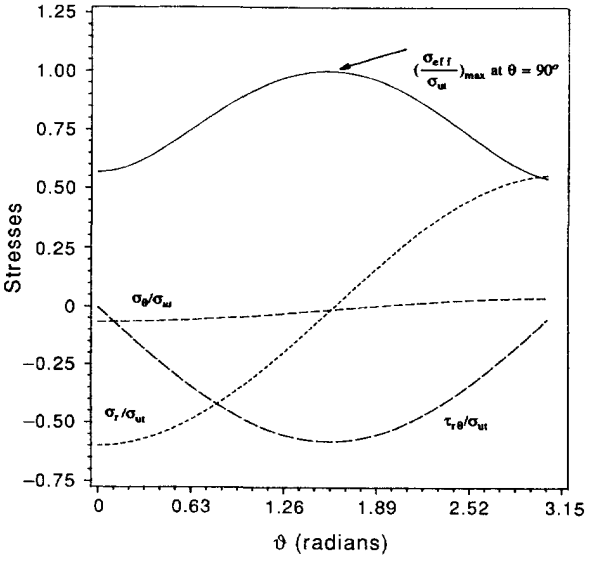

Fig. 13. Stress pattern in the half-disk. ($\gamma = 0.2$, $\bar{a}/W = 0.2$, critical speed, $\omega_c = 22{,}870$ rpm. Material: steel 4340, $K_{IC} = 144.3$ ksi $\sqrt{\text{in.}}$, $\rho = 0.28$ lb in^{-3}.)

there was no information in the reference about the number of fragments produced at the failure of a disk having a part-through radial crack propagated from the bore.

4. CONCLUSIONS

Using the plane theory of elasticity, the fragmentation of a rotating flat disk at failure has been analysed. The size and the number of pie-sector shaped fragments obtained in the analysis are compared with the available experimental results. The results are in close agreement with the experiment. The number of fragments increases as the ratio of inner to outer radii increases. This result is consistent with the experiment. The analysis is applicable to disks having smaller inside to outside radii.

Acknowledgment—The authors greatly acknowledge the computation facility provided by the School of Aerospace and Mechanical Engineering.

REFERENCES

ASTM (1987). *Metals and Mechanical Testing*; *Elevated and Low Temperature Testing*; *Metallography*. American Society for Testing and Materials, Philadelphia.

Bandera, C., Nicolich, M. and Strozzi, A. (1993). On the bursting mechanism in rotating rings. *J. Strain Anal.* **28,** 153–162.

Gdoutos, E. E. (1984). *Problems of Mixed Mode Crack Propagation*. Martinus Nijhoff, Boston, MA.

Köhl, M. and Dhondt, G. (1993). Failure analysis of aircraft engine disks. *Int. J. Solids Struct.* **30,** 137–149.

Mangano, G. J. (1975). Studies of engine rotor fragment impact on protective structure. AGARD-CP-186.

McCarthy, D. (1975). Definition of engine debris and some proposals for reducing potential damage to aircraft structure. AGARD-CP-186.

Metals Handbook (1990). Vol. 1. ASM International, Metals Park, OH.

Sakata, M., Aoki, S., Kanzawa, M., Ogure, N. and Tateishi, K. (1978). *J*-integral approach to fracture of rotating disks. *J. Engng Mater. Technol.* **100,** 128–133.

Sakata, M., Aoki, S., Kishimoto, K., Kanzawa, M. and Ogure, N. (1985). Crack growth and instable fracture of rotating disks. *J. Engng Mater. Technol.* **107,** 154–160.

Sato, Y. and Nagai, F. (1963a). Strength of rotating disks of brittle material like cast iron. National Aerospace Laboratory, Tokyo, Japan, NAL TR-38 (in Japanese).

Sato, Y. and Nagai, F. (1963b). Influence of coriolis force on the burst of rotating disk of cast iron. National Aerospace Laboratory, Tokyo, Japan, NAL TR-47 (in Japanese).

Williams, M. L. (1974). On the mathematical criterion for fracture. In *Thin Shell Structures* (Edited by Y. C. Fung and E. E. Sechler), pp. 467–481. Prentice-Hall, Englewood Cliffs, NJ.